Quantitative super-resolution microscopy reveals distinct ULK1 oligomeric states and nanoscopic morphologies during autophagy initiation

Chiranjib Banerjee[1], Daihyun Song[2], Dushyant Mehra[1,3], Angel Mancebo[1], Do-Hyung Kim[2,*] and Elias M. Puchner[1,*]

1. School of Physics and Astronomy, University of Minnesota, Twin Cities
2. Department of Biochemistry, Molecular Biology, and Biophysics, University of Minnesota, Twin Cities
3. Department of Biomedical Engineering and Physiology, Mayo Clinic, Rochester, MN

[*] Corresponding authors: epuchner@umn.edu and dhkim@umn.edu

Abstract

Autophagy is an evolutionarily conserved process for degradation and recycling of intracellular components. Although autophagy has been extensively studied over the past decades, it still remains unclear how autophagosome formation occurs in response to starvation. Here, using quantitative Photoactivated Localization Microscopy (qPALM) we have analyzed the nanoscopic spatial distribution and the oligomeric states of endogenous ULK1, the central autophagy induction regulator. For this, we introduced the gene of mEos2, a photoswitchable fluorescent protein, into the ULK1 allele of the HeLa cell genome using a genome-editing technique to express mEos2-ULK1 at an endogenous level. With single-molecule sensitivity, we found that ULK1 exists as various oligomers with clustered and arc-shaped structures throughout the cytoplasm. Upon induction of autophagy by amino acid starvation, a small fraction of ULK1 molecules formed higher-order oligomers localized to larger spherical structures with radii up to 380 nm. Cross-correlation analysis of two-color PALM data of ULK1 and its interaction partner Atg13 revealed that ULK1 structures composed of more than ~40 molecules form under starvation only when ULK1 and Atg13 are colocalized. Through two-color PALM analysis of ULK1 and the endoplasmic reticulum (ER) compartment, we found that these autophagic ULK1 structures occur in a close proximity of the ER within 800 nm. These results indicate that ULK1 might engage in the initiation of autophagosome formation at and near the ER where its cluster size expands to contain more than 40 ULK1 molecules. This quantitative analysis of endogenous ULK1 has provided unprecedented insights into the origin of the autophagy initiation structures.

Keywords: Autophagy, ULK1, Atg13, PALM/STORM, single molecule sensitivity, photoswitchable fluorescent protein, cross correlation, CRISPR/Cas9, endogenous tagging.

Significance Statement

Despite extensive research over the past decades, the molecular mechanism for autophagy initiation remains obscure. Here, we applied Photoactivation Localization Microscopy techniques, coupled with genome-editing, to quantify the oligomeric states and nanoscale behaviors of endogenous ULK1, the central autophagy regulator. The quantitative PALM analysis revealed that ULK1 forms high order multimeric clusters containing up to ~60 molecules, and the oligomeric states increase in response to amino acid starvation up to ~190 molecules. Through cross-correlation analysis, we identified a threshold number of ULK1 molecules that might reflect the state of ULK1 engaging in autophagy initiation in close proximity to the endoplasmic reticulum. These results have provided an unprecedented level of insight into the molecular behavior of ULK1 during autophagy initiation.

Introduction

Macroautophagy (hereafter referred to as autophagy) is an evolutionarily conserved process in eukaryotic cells that degrades intracellular organelles and macromolecules in the lysosome. Autophagy plays a fundamental role in maintaining the balance between production, degradation, and recycling of cellular constituents. Dys-regulation of autophagy is closely related to various diseases, such as cancer, neurodegeneration, and diabetes (1, 2). Autophagy is mainly induced under starvation of amino acids or other harsh stress conditions via suppression of mechanistic target of rapamycin complex 1 (mTORC1), the central nutrient-sensitive protein kinase complex (3-5). Despite the recent progress in our understanding of autophagy, the exact mechanism of autophagy initiation remains unclear. Autophagy initiates with the formation of an autophagosome, the double membrane structure that encompasses its cargo. The key step for the induction of autophagosome formation is activation of the UNC51-like kinase 1 (ULK1) (6-9). How exactly ULK1 engages to initiate autophagosome formation remains poorly understood.

ULK1 forms a large protein complex by interacting with Atg13, FIP200 (FAK family kinase interacting protein 200 kDa), and Atg101 (6-13). Previous studies have shown that ULK1 forms puncta in the cytoplasm in starved cells as an early event for the formation of the phagophore, the precursor membrane structure for the autophagosome (14, 15). A recent study has shown that the ULK1 complex exists on the endoplasmic reticulum (ER) and Atg9 compartments. It was shown that the formation of phagophores occurs at the ER-mitochondria contact sites or on the surface of the mitochondria (16, 17). Furthermore, Biazik et al. (18) has shown that the membrane contacts of the phagophores occur extensively with the membranes from putative ER exit sites, late endosomes or lysosomes, and the Golgi complex as well as mitochondria. These studies have relied on confocal or other conventional fluorescence microscopy techniques. However, due to the limited resolution of those microscopy techniques, the exact location of ULK1, the size of the initiation complexes and the number of ULK1 molecules required to initiate the phagophore formation have remained unclear.

The emergence of the highly sensitive molecular imaging techniques over the past decade, such as single-molecule localization microscopy techniques(19, 20), has made it possible to resolve intracellular structures below the optical diffraction limit (21). In particular, quantitative

Photoactivated Localization Microscopy (qPALM) (20, 22) using irreversibly bleaching photoconvertible or photoswitchable fluorescent proteins (PSFPs) has enabled us to count the number of molecules in diffraction limited structures. Several recent studies have made progress in quantifying the number of single molecules with PALM by correcting for blinking of PSFPs (20, 22-25). Approaches, such as pair-correlation analysis, have been employed to quantify average spatial distribution of signaling proteins (26, 27). Jungmann et al. (28) were able to quantify the number of molecules based on the 'on-off' binding of fluorophores labeled with small DNA oligomers. DNA origami has also been developed into a calibration standard for quantifying the number of molecules in mammalian cells (29, 30).

The application of qPALM to mammalian proteins requires tagging a protein of interest with a PSFP. Most fluorescence and super-resolution microscopy studies in mammalian cells have been based on overexpression of fluorescently tagged proteins (31). However, overexpression can cause artifacts for determining the oligomeric state and spatial distribution of proteins (32). In addition, overexpression can abnormally alter the biological function of proteins (33). Previously, four studies have applied PALM with endogenously tagged proteins (34-37). However, none of the studies have quantified the number of proteins due to the challenges for single-molecule counting caused by the blinking behavior of PSFPs.

In this study, we have employed a genome-editing technique to express endogenous ULK1 as a fusion with mEos2, a PSFP, by introducing the gene of mEos2 into the ULK1 gene allele in the HeLa cell genome. By applying qPALM to the genetically modified cells, we have determined the nanoscopic distribution and the oligomeric state of endogenous ULK1 with single-molecule sensitivity. Through two-color PALM and cross-correlation analysis, we were able to quantify a threshold number of ULK1 molecules that might reflect the state of ULK1 participating in autophagy initiation. These results have provided an unprecedented level of quantitative insight into ULK1 multimerization and cellular distribution during autophagy initiation.

Results

Quantitative analysis of endogenous ULK1 clusters using qPALM

ULK1 has previously been shown to form puncta in the cytoplasm as an early event that occurs prior to autophagosome formation(14, 15, 38, 39). However, the mechanism underlying ULK1 puncta formation and how ULK1 puncta engage in autophagosome formation remain unknown. Characterizinig the nature and function of ULK1 puncta is critical to better understand how autophagosome formation is initiated. To this end, we employed qPALM to quantify the multimeric states and nanoscopic distribution of ULK1 molecules. To avoid alteration of the biological function and counting artifacts for qPALM caused by overexpression, we engineered the genome of HeLa cells to express endogenous ULK1 as a fusion with mEos2 by the CRISPER/Cas9-assisted genome editing technique (40) (Fig. 1A). We selected genome-edited cells in which every endogenous ULK1 was expressed as a fusion with mEos2 (Fig. 1B). The endogenously tagged ULK1 interacted with Atg13 and FIP200 as similarly as untagged endogenous ULK1 (Fig. 1B), and it responded to amino acid starvation for its activation toward phosphorylation of Atg14 Ser29, an ULK1 target site (15) (Fig. 1C). The genome-edited cells showed similar numbers of Atg13 and LC3B puncta as unmodified original HeLa cells under amino acid starvation (Fig. S1). These results demonstrate that the functional properties of ULK1 have not been disturbed by the genome editing.

Using the genome-edited cells, we recorded PALM images of mEos2-ULK1 using 405 nm as a photoactivation wavelength. We used very low intensities of photoactivation light to avoid spatio-temporal overlap of the signals from single mEos2 molecules (Fig. S2A-C). By applying the radial distribution (or pair-correlation) analysis (20, 22), we determined that the maximum spread of fluorescent bursts originating from single mEos2-ULK1 molecules is 80 nm (Fig. S2D). This is equivalent to the largest localization uncertainty in raw PALM images (20). Next, we grouped localizations appearing from the same mEos2-ULK1 molecules within a distance of 80 nm, and obtained a histogram of dark times from single mEos2 emitters (Fig. S2E). By integrating and normalizing the dark-time histogram, we determined the dark time cutoff, within which 99% of fluorescent bursts from single mEos2 molecules appear. (Fig. S2F). The dark time cutoff of mEos2-ULK1 was 4.5 s in our experimental conditions. This cutoff time is similar to a recently

reported value of 4.1 s in HeLa cells at a 99.8% cutoff (41). While other studies reported a 99% dark-time cutoff of mEos2 of 2.66 in yeast (20) and 6.4 s in mammalian cells (22), it is important to note that this value depends on the imaging conditions and does not significantly alter the result due to the flatness of the integrated dark time histogram at high percentiles (Fig. S2). Using the dark-time parameter and the spatial spread of localizations, we corrected the PALM data to obtain the actual local number of ULK1 molecules in ULK1 clusters with ~20 nm resolution as well as the overall distribution of oligomeric states within a cell (Fig. 1D and E).

Transiently overexpressed ULK1 behaves differently from endogenous ULK1 in the nanoscopic distribution and oligomeric state.

Super-resolution and conventional fluorescence imaging experiments have been prevalently performed with proteins overexpressed in mammalian cells. Because overexpression can disturb the stoichiometry of protein compositions in complexes or pathways, using overexpressed proteins can produce misguiding results. By comparing PALM images between endogenously tagged mEos2-ULK1 and overexpressed mEos2-ULK1, we found that the sizes and intensities of ULK1 puncta were more heterogeneous and larger in ULK1-overexpressing cells (Fig. 2A). By applying qPALM analysis, we counted the number of proteins in ULK1 clusters and found that overexpressed ULK1 exhibits a different pattern of multimerization from that of endogenous ULK1 (Fig. 2B and C). Endogenous ULK1 formed clusters containing a significantly lower number of molecules compared to overexpressed ULK1. Through the pair-correlation function analysis, which quantifies the distribution of distances between all pairs of localizations (26), we determined that the average distance of ULK1 molecules in clusters was significantly larger with overexpressed ULK1 (Fig. 2C). Although endogenously tagged ULK1 is less abundant in cells compared to its overexpressed form, its clusters smaller than 30 nm exhibited a higher density of ULK1 (Fig. 2C). This indicates that overexpressed ULK1 might have a reduced competence to form high density clusters. Combined, these results suggest that overexpressed ULK1 behaves differently from endogenous ULK1 in forming the oligomeric states.

Amino acid starvation induces large high-order ULK1 oligomers

Having established qPALM for endogenous ULK1, we asked how amino acid starvation affects the oligomeric state of ULK1. Regardless of amino acid supplementation, ULK1 was mainly

distributed throughout the cytoplasm (Fig. 3A and B). Over 95% of ULK1 molecules existed as clusters containing less than 10 molecules in either amino acid supplemented or depleted condition. In amino acid starved cells, we observed emergence of arc-shaped and spherical structures of various sizes that could not be resolved in conventional fluorescence images (Fig. 3B). Analysis of the oligomeric states revealed that a large population of ULK1 exists as multimeric states containing 1-to-60 molecules in amino acid-supplemented cells (Fig. 3C). In amino acid deprivation, ULK1 formed in addition higher-order multimeric clusters consisting of 60-190 ULK1 molecules, which have not been detected in amino acid supplemented cells.

To further clarify how amino acid starvation affects ULK1 clusters, we conducted the pair-correlation analysis. The majority of ULK1 structures with diameter less than 30 nm formed much denser clusters in both amino acid fed and starved cells (Fig. 3D). However, the pair-correlation magnitude was higher in starved cells compared to fed cells at distances larger than 30 nm, corroborating the observation that amino acid starvation induces the formation of larger structures with a larger number of ULK1 molecules. Combined, these results indicate that while ULK1 is present as multimeric clusters with varying stoichiometry, morphology and size in both fed and starved conditions, amino acid starvation induces the formation of larger structures with a larger number of ULK1 molecule.

ULK1 structures containing Atg13 display variability in size, shape and multimeric state

We wondered whether the different pattern of ULK1 multimeric states in fed and starved cells can provide any clue about the specific type of ULK1 clusters that engage in the initiation of autophagosome formation. To answer this question, we performed two-color co-localization PALM experiments monitoring both ULK1 and Atg13, a critical binding partner of ULK1 (6-8). We hypothesized that if the structures with high order multimeric states induced by amino acid starvation are related to autophagy, they should co-localize with Atg13. To address the hypothesis, we transiently expressed Atg13 as a fusion with HaloTag in mEos2-ULK1-expressing HeLa cells. HaloTag covalently binds to organic fluorophore ligands in a one to one ratio producing high photon counts (and thus high localization precision) (42, 43). We used JF646 dye as a HaloTag ligand, which has no spectral overlap with mEos2 to generate PALM images (Fig 4A). In fed cells, both Atg13 and ULK1 formed small clusters that were distributed throughout the cytoplasm (Fig

4A, left). Starved cells also contained small ULK1 clusters that did and did not co-localize with Atg13. However, starvation induced in addition larger arc-shaped and spherical structures that contained both ULK1 and Atg13 (Fig. 4A, right). Two-color PALM analysis showed that ULK1 clustering pattern is different between those that colocalized with Atg13 and those that did not colocalize with Atg13. Interestingly, ULK1 structures associated with Atg13 exhibited variability in size, shape, and multimeric state, which included small, dense ULK1 clusters as well as larger structures composed of various oligomeric states of ULK1 (Fig. 4B, left). In contrast, ULK1 clusters that did not co-localize with Atg13 only formed small clusters (Fig. 4B, right).

To further clarify the nature of ULK1 clusters that co-localize with Atg13, we performed cross-correlation analysis (27, 44) of single-molecule localizations of ULK1 and Atg13 in fed and starved cells. In both conditions, we observed a pronounced peak of the cross-correlation at short distances up to 100 nm; however, under starvation the peak was significantly higher and broader up to 200 nm (Fig. 4C). This result implies a more significant extent of co-localization between ULK1 and Atg13 in enlarged structures that might be relevant to the initiation of autophagy.

Cross-correlation analysis identified Atg13-containing structures with up to 190 ULK1 molecules under starvation.

Based on the cross-correlation result, we separately analyzed the ULK1 molecules that have a distance of less than 100 nm to Atg13 and all other ULK1 molecules (Fig. 5A). Those ULK1 molecules within 100 nm of Atg13 are considered to be in close proximity or interact with Atg13 in both fed and starved cells as seen in the previous cross-correlation (Fig. 4C). We then analyzed the size and number of ULK1 molecules inside and outside Atg13-containing structures. In fed cells, structures containing Atg13 had up to 47 ULK1 molecules with a mean of 34.9 ± 5 (mean ± SD), whereas structures without Atg13 contained up to 56 ULK1 molecules with a mean 42.7 ± 9.9, (Fig. 5B, see also Materials and Methods and Supplemental information). There was no detectable difference in the sizes of the two types of structures.

The same analysis of amino acid starved cells revealed a dramatically different result. Structures without Atg13 had no detectable difference in the number of ULK1 molecules and sizes compared to fed cells (Fig. 5B). In contrast, some Atg13-containing structures contained significantly more

than 40 ULK1 molecules up to 190 ULK1 molecules under starvation (Fig. 3C and Fig. 5B). The scatter plot of the number of ULK1 molecules vs. size of structures revealed that starved cells contained an average of 8 structures containing both Atg13 and more than 40 molecules per cell, whereas only 0.6 were detected in fed cells (Fig 5C).We also compared the distribution of radii of structures in starved cells that contain Atg13 with more than 40 and less than 40 ULK1 molecules as well as structures without Atg13 (Fig. 5E). Structures without Atg13 had a roughly constant probability near up to ~200 nm of radius, whereas structures containing Atg13 and less than 40 ULK1 molecules exhibited a peak approximately at 200 nm with a tail up to 300 nm (Fig. 5D). Structures containing Atg13 with more than 40 ULK1 molecules exhibited the largest radii up to 380 nm. The radial distribution analysis of the same classes of structures revealed that ULK1 molecules without Atg13 formed smallest clusters with a low ULK1 density of 100 molecules/μm^2 (Fig. 5E). Structures with Atg13 but less than 40 ULK1 molecules formed the densest clusters up to 300 molecules/μm^2. Interestingly Atg13 containing structures with more than 40 ULK1 molecules had again a lower density but a long tail reflecting their larger size. This result demonstrates that initially dense ULK1 clusters with Atg13 disintegrate on larger Atg13 containing structures with more than 40 ULK1 molecules. These results demonstrate that our cross-correlation analysis could identify unique Atg13- and ULK1-containing structures that are induced by starvation.

Two-color cross-correlation analysis reveals large ULK1 structures in the proximity to the ER

In order to more clearly assess where the large structures containing ≥ 40 ULK1 molecules emerge, we performed co-localization PALM experiments with endogenously tagged mEos2-ULK1 and the transiently expressed ER marker HaloTag-Sec61β bound with JF646. ULK1 was visually localized on or near the tubular ER regions but also to some extent throughout the cytoplasm in both fed and starved cells (Fig. 6A). In starved cells, large ULK1 clusters not present in fed cells were in contact or close to the ER (Fig. 6A, lower right). To quantify the extent of the ER localization of the large ULK1 structures with more than 40 molecules, we performed the cross-correlation analysis. The cross-correlation plot showed a strong co-localization of the ER and ULK1 structures up to a distance of about 800 nm (Fig. 6B). At distances larger than 800 nm, the magnitude of the cross-correlation plot was flattened and close to 1, implying no accumulation of

ULK1 structures beyond this distance from the ER. This result suggests that ULK1 molecules likely engaging in autophagy are localized to and near the ER where they accumulate to form dense clusters and larger structures of >40 molecules. These structures might develop into the phagophores in proximity to the ER (Fig. 6C).

Discussion

In this study, we have characterized the spatial distribution and oligomeric states of endogenous ULK1 at the single-molecule level with 20 nm spatial resolution. Our study showed that overexpressed ULK1 behaves differently from endogenous ULK1 in forming the oligomeric states. This result, in addition to multiple potential issues associated with overexpression studies, led us to perform the quantitative PALM analysis for endogenous ULK1. Our study is not the first in applying PALM approaches for endogenously tagged proteins (34-37). However, none of the studies was able to quantify the number of proteins due to the challenges for single-molecule counting caused by the blinking behavior of the PSFP. Several recent studies have made progress in quantifying the number of single molecules by correcting for fluorophore blinking (20-25). However, they have not yet been performed with endogenously tagged proteins. Therefore, this study is the first in the cell biology field quantifying endogenous proteins in multimerization and their nanoscopic spatial distribution in cells.

The PALM quantification approach we have employed is based on grouping localizations from the same fluorophore within a spatio-temporal threshold (20, 41). A challenge for this quantification is that PSFPs do not emit at a constant intensity until they bleach but rather exhibit a variable number of fluorescent bursts separated by a variable time. This phenomenon causes single PSFPs to appear as clusters with a variable number of localizations (20, 27, 45). To quantify the oligomeric states of a protein of interest with this qPALM approach, the PSFP must meet two requirements: First, the PSFP must irreversibly bleach within a short time compared to the entire imaging sequence; Second, the distribution of dark times between fluorescent bursts of single PSFP must be known. Since the photophysical properties of PSFPs strongly depend on the properties of the environment as well as experimental conditions, both spatio- and temporal thresholds for grouping localizations should be determined under the same imaging conditions as

the actual experiment. By performing PALM experiments at a very low 405 nm power to avoid the spatio-temporal overlap of PSFPs, we determined the dark time distribution of mEos2 and a dark-time cutoff of 4.5 s that covers 99% of localizations (Fig. S2). While other studies employed different cutoff times(20, 22, 41), we note that the cumulative dark time distribution at such long times is flat and a variation by 1.5 s results in only 1% change of the covered localizations.

By applying this qPALM approach, we were able to characterize the behaviors of endogenous ULK1 during autophagy initiation at an unprecedented molecular resolution. We found that ULK1 forms clusters with up to 60 molecules in fed conditions. Starvation induced a small fraction of ULK1 structures containing a higher number up to 190 ULK1 molecules. To discriminate ULK1 structures induced under starvation from the basally existing ones in fed cells, we performed co-localization with its interaction partner Atg13. ULK1 that colocalized with Atg13 formed structures of small dense clusters as well as arc and spherical morphologies in starved conditions (Fig. 3 and 4). These Atg13-colocalizing structures were not found in fed cells. ULK1 that did not colocalize with Atg13 was not able to form such highly dense clusters of ULK1, supporting the relevance of the highly dense clusters to autophagy (Fig. 5B and 5E). Furthermore, we found arc-shaped and large spherical structures with the highest number of up to 190 ULK1 molecules in various multimeric states under starvation (Fig. 5B). These structures only formed under starvation for ULK1 molecules that colocalize with Atg13. The arc and spherical structures of ULK1 are similar to the structures described in a recent study by Karanasios et al. (38). The arc-shaped structures might be phagophores, which emerge from dense but small ULK1- and Atg13-containing clusters and become spherical structures of large sizes. Based on our result, we speculate that phagophores might form only when a critical number of ULK1 molecules (~40) containing Atg13 accumulate as a cluster.

Our cross-correlation analysis revealed that ULK1 molecules in fed and starved cells localize to the ER. Starvation-induced structures containing Atg13 and more than 40 ULK1 molecules are present on and near the ER. Because of the close proximity of ULK1 to the ER membrane, it has been difficult to discriminate the exact location of ULK1 clusters using conventional fluorescence microscopy techniques. Karanasios et al. (38) showed that the nucleation of autophagosomes occurs in regions where the ULK1 complex coalesces with the ER and the Atg9 compartment.

Biazik et al. (18) identified multiple contact sites between the phagophore and membranes from putative ER exit sites, late endosomes or lysosomes, the Golgi complex, and mitochondria. The study also showed that one phagophore could have simultaneous multiple contact sites with more than one organelle. Our two-color PALM analysis led us to identify that the ULK1 structures containing more than 40 molecules are present at distances up to 800 nm from the ER (Fig. 6C). While this result supports the prevailing notion that phagophore and autophagosome formation occurs on or near the ER, our study provides a quantitative demonstration of the ER proximity model through super-resolution imaging tools.

In summary, the application of qPALM techniques to endogenously tagged ULK1 has provided unprecedented insights into the nature and the behavior of ULK1 molecules at the initiation of autophagosome formation. Our study could not explain the molecular basis for the formation of such large clusters of ULK1 molecules and for their dynamic alteration in response to starvation. The application of qPALM for endogenous proteins can be expanded in combination with biochemical tools modulating the activity of ULK1 or other signaling molecules impinging on the autophagy initiation site to address those questions as well as many other outstanding questions in autophagy.

Materials and Methods

Generation of genome-edited cells

To introduce the fluorescence protein tag into the ULK1 locus of the genome of HeLa cells, we used the CRISPR-Cas9-assisted genome editing technique (46). The detail of the general procedure has been described in our previous report (39). The gRNA sequence (GCGGCCGGGCTCCATGGCGC) was cloned into pSpCas9(BB)-2A-GFP (Addgene, PX458; deposited by Dr. Feng Zhang). The replacement DNA was designed to contain 700 bps of the homologous region for both sides of the inserted mEos2 sequence. Four tandem repeats of GGT nucleotide sequences were added to the end of the fluorescence protein gene sequences. The gRNA plasmid and the replacement plasmid were introduced into HeLa cells using the Neon transfection system (ThermoFisher Scientific). GFP-positive cells were sorted and plated in 96-well plates as

a single cell. Cloned cells were amplified and the clones harboring the replacement were screened and confirmed by western blotting and DNA sequencing.

DNA construction

mEos2-tagged ULK1 construct and HaloTag tagged Atg13 and Sec61β constructs were prepared by PCR amplification of the genes and cloned into pCSII-mEos2 and pCSII-HaloTag plasmids derived from the pCSII-EF vector (provided by Dr. Nik Somia, University of Minnesota). Restriction enzyme sites at XhoI and NotI in the vector were used to clone mEos2 and HaloTag. These pairs of primers were used to clone the genes: 5'-gagcga**gtcgac**catgagtgcgattaagcca-3' and 5'-gagca**ctcgag**ccacctccgccacctcgtctggcattgtcag-3' for mEos2;
5'-gagcgactcgagcaccatggcagaaatcggtact-3' and
5'-gtctcgaagcggccgcattgcatacgatggtcgacccggaaatctccagcgttgacagcca-3' for HaloTag. The genes of ULK1, Atg13 and Sec61β were cloned into the mEos2 and HaloTag plasmids at SalI and NotI sites. The LC3B plasmid (Addgene #11546) was a kind gift from Dr. Karla Kirkegaard.

Co-immunoprecipitation and western blotting

The mEos2-tagged endogenous ULK1 was enriched by immunoprecipitation using an anti-ULK1 antibody (Santa Cruz Biotech., sc-10900) following the procedure we described in our previous report (7, 15, 39). We used a lysis buffer containing 40 mM HEPES, pH 7.4, 120 mM NaCl, 1 mM EDTA, 50 mM NaF, 1.5 mM Na_3VO_4, 10 mM beta-glycerophosphate, 1% Triton X-100 (Sigma-Aldrich, X100) supplemented with protease inhibitors (Roche, 05056489001). Immunoprecipitated proteins were run on Tris-glycine gels (Thermo Fisher Scientific, XP04125BOX), transferred onto immunoblot polyvinylidene difluoride (PVDF) membranes (Bio-Rad, 1620177), and detected using ECL reagents (GenDEPOT, 20-300B). The following antibodies were used for western blotting: ULK1 (sc-33182) from Santa Cruz Biotech.; p-Atg14 Ser29 (13155) and Atg14 (96752) from Cell Signaling Technology; Atg13 antibody was described in our previous report (ref_7).

Preparation of cells for imaging.

HeLa cells were maintained in fluorobrite DMEM (Invitrogen) supplemented with 10% fetal bovine serum, 4 mM glutamine (Gibco), 1 mM sodium pyruvate (Gibco) and 1% penicillin-

streptomycin antibiotics (Invitrogen) in a T25 flask. Cells were subcultured on eight-well chambered cover glasses (Cellvis, C8-1.58-N) 24 h before transfection. Transient transfections were performed using GeneJET (ThermoFisher Scientific) 12–24 h before the measurements. The transfected cells were cultured in full medium or Earle's Balanced Salt Solution (EBSS) for 150 min in the presence of 180 nM bafilomycin A1 (BAFA1). BAFA1 is widely used in the field to increase the number of detected autophagosomes in each cell by inhibiting the fusion of autophagosomes with lysosomes. All the imaging experiments have been performed in fixed cells. For fixation, cells were treated with 3% (v/v) formaldehyde for 30 min. After fixation, we used Dulbecco's phosphate-buffered saline (PBS) with calcium and magnesium (Gibco) for measurements.

For two-color imaging of mEos2-ULK1 with Atg13-HaloTag or the ER marker Sec61-HaloTag, we used the organic dyes Oregon green (OG) and JF 646 conjugated to the HaloTag ligands (Promega). Both dyes exhibit no overlap of their absorption and emission spectra with photoconverted mEos2. The dyes were added to live cells on the coverglass of the 8-well chambers at a final concentration of 500 nM for OG and 1 to 10 nM for JF 646. After an incubation time of 15-20 min cells were fixed with 3% formaldehyde and washed five times with PBS containing 1% Triton-X (TX-100) to remove access dyes that did not covalently bind to the HaloTag.

PALM and conventional fluorescence data acquisition

All microscopy experiments were performed with a Nikon Ti-E inverted microscope with a Perfect Focus System and recorded on an electron-multiplying CCD camera (Ixon89Ultra DU897U; Andor) at a frame rate of 20 Hz as described in detail in the supplemental information. In short, for PALM imaging of mEos2-ULK1 one photoactivation frame (405 nm laser, 1–251 µW corresponding to a power density of roughly 0.06–15 W/cm^2) with simultaneous transmitted light imaging was followed by nine frames of excitation (561 nm, 17 mW corresponding to a power density of roughly 1 kW/cm^2). For two-color PALM imaging of mEos2-ULK1 and HaloTag JF646, the excitation frames consisted of five 561 nm excitation frames for mEos2 followed by five 640 nm excitation frames (640 nm, 17.5 mW, roughly 1 kW/cm^2) Photoactivation and excitation cycles were repeated until all mEos2/JF646 molecules were imaged and bleached typically until a movie recorded at 20 Hz reached 8,000-15,000 frames. The point spread functions of single molecules

were then fitted with an elliptical Gaussian function using Insight3 (Zhuang lab, http://zhuang.harvard.edu/software.html) to determine their centroid positions, intensities, widths, and ellipticities. For all localizations, the x and y coordinates, photon number, background photons, width, the frame of appearance, and other fit parameters were saved in a molecule list for further analysis. To correct for drift, all molecule lists were drift corrected using the repetitive transmitted light images (47). The conventional fluorescence images were generated by averaging the 50 frames (Fig. S1) and 500 frames for Fig. 3A recorded at 20 Hz with a 488 nm excitation power density of 0.085 W/cm2.

Quantitative analysis of molecule numbers

Once a single mEos2 molecule is stochastically photoactivated, it emits a variable number of fluorescent bursts that are separated by a variable dark time until irreversible bleaching occurs. These fluorescent bursts can be combined since the 405 nm photoactivation rate was kept low enough to avoid spatio-temporal overlap with a nearby mEos2 molecule. The combination of these fluorescent bursts is based on two thresholds: 1) a distance threshold that specifies the maximum separation of fluorescent bursts from a mEos2 molecule (corresponding to the localization precision) and 2) a temporal dark-time threshold that specifies the maximum time between fluorescent bursts from a mEos2 molecule. The distance threshold was measured using the pair-correlation function (Fig. S2D), which revealed that fluorescent bursts from single mEos2 molecules are spatially separated by less than 80 nm. The dark-time threshold was determined from the cumulative dark-time histogram of fluorescent bursts and set to 4.5 seconds, which covers 99% of the dark times (Fig S2E and F). Based on these two parameters, a custom written Matlab procedure combines two localizations from fluorescent bursts to a photon-weighted average position if they are separated by less than 80 nm and less than 4.5s. If a third localization again appears within the cutoff time with respect to the preceding one and within 80 nm compared to the averaged position of the previous two localizations, a new photon-weighted average position is calculated from the three localizations. This iterative process is repeated until all localizations from the same mEos2 molecules are combined to a photon weighted average position. The average position has a higher localization precision due to the increased number of photons. From the resulting blink-corrected molecule list, the actual number of mEos2 molecules and their spatial distribution can be further analyzed.

To count the number of ULK1 molecules in initiation complexes and forming autophagosomal structures in an unbiased way, we determined their size distribution in the amino acid starved conditions using the pair-correlation function of the blink-corrected mEos2 molecule list. Based on the peak of the pair correlation function up to 600 nm, ULK1 molecules within a radius of 300 nm were therefore assigned to one cluster.

Alignment of two-color PALM data.

To superimpose two color PALM data for images or cross correlation analysis, we recorded conventional fluorescence images of fluorescent beads (TetraSpeck microspheres, Invitrogen T7279) that were excited at 561 nm and 640 nm and appeared in both channels. The transformation between the two channels across the field of view was then obtained by localizing individual beads in both channels and by determining the 3rd order polynomial transformation between their coordinates. The accuracy of the transformation was then verified by recording a different field of view of fluorescent beads and superimposing both channels using the determined transformation. As seen in Fig. S3, the deviation of the bead locations from both channels was less than 19 nm, which is smaller than the localization precision of PALM.

Spatial Cross-Correlation analysis and cluster identification

After identification of blink corrected ULK1 molecules, molecules were assigned to clusters. The radial distribution (or pair correlation) among all blink corrected molecules was calculated and molecules that were within 400 nm of each other were identified as ULK1 clusters. The obtained partial radial distribution function was normalized by the number of molecules in both datasets and the area of the field of view (27). Next, a spatial cross-correlation between the blink corrected ULK1 molecules and Atg13 localizations was performed to determine the distance distribution between the two proteins. Due to the large number of localizations in both the blink corrected ULK1 and the Atg13 localization datasets, we set a 2 µm cutoff in the nearest neighbor search, which only requires 20-40 GB of working memory. This method allows for the identification of molecule pairs within a specified distance distribution across the entire desired field of view for many movies using available computational resources (analysis code was written in MATLAB 2018b and run on an Alienware Aurora G6 computer with 3.80 GHz CPU, 40 GB of

working memory, NVIDIA GeForce GTX 1070 8 GB graphics card, and 900 GB of disk space). Next, ULK1 clusters that contained at least one ULK1 molecule within 100 nm of an Atg13 localization (labelled "inside") were segregated from ULK1 clusters with no molecules within 100 nm of an Atg13 localizations (labeled " outside"). Clusters properties for inside and outside clusters such as the radius (estimated with the standard deviation of localizations in x and y) and the number of ULK1 molecules were determined separately for a comparison of fed and starved cells. This cross-correlation analysis was also applied to ULK1 molecules and ER localizations.

Estimating radii of structures:

To estimate the radius of the ULK1 clusters, the x and y positions of the molecules inside the cluster were averaged to find the center and the distance between each molecule and the center was calculated. The mean of the distances was used to approximate the radius of the ULK1 cluster.

Acknowledgment:

Research reported in this publication was supported by the National Institute of General Medical Sciences of the National Institutes of Health under Award number R21GM127965 (E.M.P) and R35GM130353 (D.H.K)

References

1. B. Levine, G. Kroemer, Autophagy in the pathogenesis of disease. *Cell* **132**, 27-42 (2008).
2. N. Mizushima, B. Levine, Autophagy in mammalian development and differentiation. *Nature cell biology* **12**, 823-830 (2010).
3. T. Noda, Y. Ohsumi, Tor, a phosphatidylinositol kinase homologue, controls autophagy in yeast. *Journal of Biological Chemistry* **273**, 3963-3966 (1998).
4. Y. Kamada, T. Sekito, Y. Ohsumi, "Autophagy in yeast: ATOR-mediated response to nutrient starvation" in TOR. (Springer, 2004), pp. 73-84.
5. C. H. Jung, S.-H. Ro, J. Cao, N. M. Otto, D.-H. Kim, mTOR regulation of autophagy. *FEBS letters* **584**, 1287-1295 (2010).
6. I. G. Ganley *et al.*, ULK1· ATG13· FIP200 complex mediates mTOR signaling and is essential for autophagy. *Journal of Biological Chemistry* **284**, 12297-12305 (2009).
7. C. H. Jung *et al.*, ULK-Atg13-FIP200 complexes mediate mTOR signaling to the autophagy machinery. *Molecular biology of the cell* **20**, 1992-2003 (2009).
8. N. Hosokawa *et al.*, Nutrient-dependent mTORC1 association with the ULK1–Atg13–FIP200 complex required for autophagy. *Molecular biology of the cell* **20**, 1981-1991 (2009).
9. C. A. Mercer, A. Kaliappan, P. B. Dennis, A novel, human Atg13 binding protein, Atg101, interacts with ULK1 and is essential for macroautophagy. *Autophagy* **5**, 649-662 (2009).
10. T. Hara *et al.*, FIP200, a ULK-interacting protein, is required for autophagosome formation in mammalian cells. *The Journal of cell biology* **181**, 497-510 (2008).
11. Y.-Y. Chang, T. P. Neufeld, An Atg1/Atg13 complex with multiple roles in TOR-mediated autophagy regulation. *Molecular biology of the cell* **20**, 2004-2014 (2009).
12. E. Y. W. Chan, A. Longatti, N. C. McKnight, S. A. Tooze, Kinase-inactivated ULK proteins inhibit autophagy via their conserved C-terminal domains using an Atg13-independent mechanism. *Molecular and cellular biology* **29**, 157-171 (2009).
13. C. A. Lamb, T. Yoshimori, S. A. Tooze, The autophagosome: origins unknown, biogenesis complex. *Nature reviews Molecular cell biology* **14**, 759-774 (2013).
14. E. Itakura, N. Mizushima, Characterization of autophagosome formation site by a hierarchical analysis of mammalian Atg proteins. *Autophagy* **6**, 764-776 (2010).
15. J.-M. Park *et al.*, The ULK1 complex mediates MTORC1 signaling to the autophagy initiation machinery via binding and phosphorylating ATG14. *Autophagy* **12**, 547-564 (2016).
16. D. W. Hailey *et al.*, Mitochondria supply membranes for autophagosome biogenesis during starvation. *Cell* **141**, 656-667 (2010).
17. M. Hamasaki *et al.*, Autophagosomes form at ER–mitochondria contact sites. *Nature* **495**, 389-393 (2013).
18. J. Biazik, P. Ylä-Anttila, H. Vihinen, E. Jokitalo, E.-L. Eskelinen, Ultrastructural relationship of the phagophore with surrounding organelles. *Autophagy* **11**, 439-451 (2015).
19. H. Shroff, H. White, E. Betzig, Photoactivated localization microscopy (PALM) of adhesion complexes. *Curr Protoc Cell Biol* **Chapter 4**, Unit 4.21 (2008).

20. E. M. Puchner, J. M. Walter, R. Kasper, B. Huang, W. A. Lim, Counting molecules in single organelles with superresolution microscopy allows tracking of the endosome maturation trajectory. *Proceedings of the National Academy of Sciences* **110**, 16015-16020 (2013).
21. S. Manley, J. M. Gillette, J. Lippincott-Schwartz, "Single-particle tracking photoactivated localization microscopy for mapping single-molecule dynamics" in Methods in enzymology. (Elsevier, 2010), vol. 475, pp. 109-120.
22. B. Van Lengerich, C. Agnew, E. M. Puchner, B. Huang, N. Jura, EGF and NRG induce phosphorylation of HER3/ERBB3 by EGFR using distinct oligomeric mechanisms. *Proceedings of the National Academy of Sciences* **114**, E2836-E2845 (2017).
23. S.-H. Lee, J. Y. Shin, A. Lee, C. Bustamante, Counting single photoactivatable fluorescent molecules by photoactivated localization microscopy (PALM). *Proceedings of the National Academy of Sciences* **109**, 17436-17441 (2012).
24. P. Annibale, S. Vanni, M. Scarselli, U. Rothlisberger, A. Radenovic, Quantitative photo activated localization microscopy: unraveling the effects of photoblinking. *PloS one* **6**, e22678 (2011).
25. J. Gunzenhäuser, N. Olivier, T. Pengo, S. Manley, Quantitative super-resolution imaging reveals protein stoichiometry and nanoscale morphology of assembling HIV-Gag virions. *Nano letters* **12**, 4705-4710 (2012).
26. P. Sengupta *et al.*, Probing protein heterogeneity in the plasma membrane using PALM and pair correlation analysis. *Nature methods* **8**, 969-975 (2011).
27. S. L. Veatch *et al.*, Correlation functions quantify super-resolution images and estimate apparent clustering due to over-counting. *PloS one* **7**, e31457 (2012).
28. R. Jungmann *et al.*, Quantitative super-resolution imaging with qPAINT. *Nature methods* **13**, 439-442 (2016).
29. F. C. Zanacchi *et al.*, A DNA origami platform for quantifying protein copy number in super-resolution. *Nature methods* **14**, 789 (2017).
30. F. C. Zanacchi, C. Manzo, R. Magrassi, N. D. Derr, M. Lakadamyali, Quantifying protein copy number in super resolution using an imaging-invariant calibration. *Biophysical journal* **116**, 2195-2203 (2019).
31. R. S. Erdmann *et al.*, Labeling strategies matter for super-resolution microscopy: a comparison between HaloTags and SNAP-tags. *Cell chemical biology* **26**, 584-592 (2019).
32. L. Ripaud *et al.*, Overexpression of Q-rich prion-like proteins suppresses polyQ cytotoxicity and alters the polyQ interactome. *Proceedings of the National Academy of Sciences* **111**, 18219-18224 (2014).
33. T. J. Gibson, M. Seiler, R. A. Veitia, The transience of transient overexpression. *Nature methods* **10**, 715-721 (2013).
34. W.-K. Cho *et al.*, Super-resolution imaging of fluorescently labeled, endogenous RNA Polymerase II in living cells with CRISPR/Cas9-mediated gene editing. *Scientific reports* **6**, 35949 (2016).
35. A. O. Khan, V. A. Simms, J. A. Pike, S. G. Thomas, N. V. Morgan, CRISPR-Cas9 mediated labelling allows for single molecule imaging and resolution. *Scientific reports* **7**, 1-9 (2017).
36. A. S. Hansen, I. Pustova, C. Cattoglio, R. Tjian, X. Darzacq, CTCF and cohesin regulate chromatin loop stability with distinct dynamics. *Elife* **6**, e25776 (2017).

37. A. O. Khan *et al.*, Optimised insert design for improved single-molecule imaging and quantification through CRISPR-Cas9 mediated knock-in. *Scientific reports* **9**, 1-13 (2019).
38. E. Karanasios *et al.*, Autophagy initiation by ULK complex assembly on ER tubulovesicular regions marked by ATG9 vesicles. *Nature communications* **7**, 1-17 (2016).
39. J.-M. Park *et al.*, ULK1 phosphorylates Ser30 of BECN1 in association with ATG14 to stimulate autophagy induction. *Autophagy* **14**, 584-597 (2018).
40. L. Cong *et al.*, Multiplex genome engineering using CRISPR/Cas systems. *Science* **339**, 819-823 (2013).
41. N. Durisic, L. Laparra-Cuervo, Á. Sandoval-Álvarez, J. S. Borbely, M. Lakadamyali, Single-molecule evaluation of fluorescent protein photoactivation efficiency using an in vivo nanotemplate. *Nature methods* **11**, 156-162 (2014).
42. H. A. Benink, M. Urh, "HaloTag technology for specific and covalent labeling of fusion proteins" in Site-Specific Protein Labeling. (Springer, 2015), pp. 119-128.
43. C. G. England, H. Luo, W. Cai, HaloTag technology: a versatile platform for biomedical applications. *Bioconjugate chemistry* **26**, 975-986 (2015).
44. M. B. Stone, S. L. Veatch, Steady-state cross-correlations for live two-colour super-resolution localization data sets. *Nature communications* **6**, 1-10 (2015).
45. R. Berardozzi, V. Adam, A. Martins, D. Bourgeois, Arginine 66 controls dark-state formation in green-to-red photoconvertible fluorescent proteins. *Journal of the American Chemical Society* **138**, 558-565 (2016).
46. P. D. Hsu, E. S. Lander, F. Zhang, Development and applications of CRISPR-Cas9 for genome engineering. *Cell* **157**, 1262-1278 (2014).
47. R. McGorty, D. Kamiyama, B. Huang, Active microscope stabilization in three dimensions using image correlation. *Optical nanoscopy* **2**, 3 (2013).

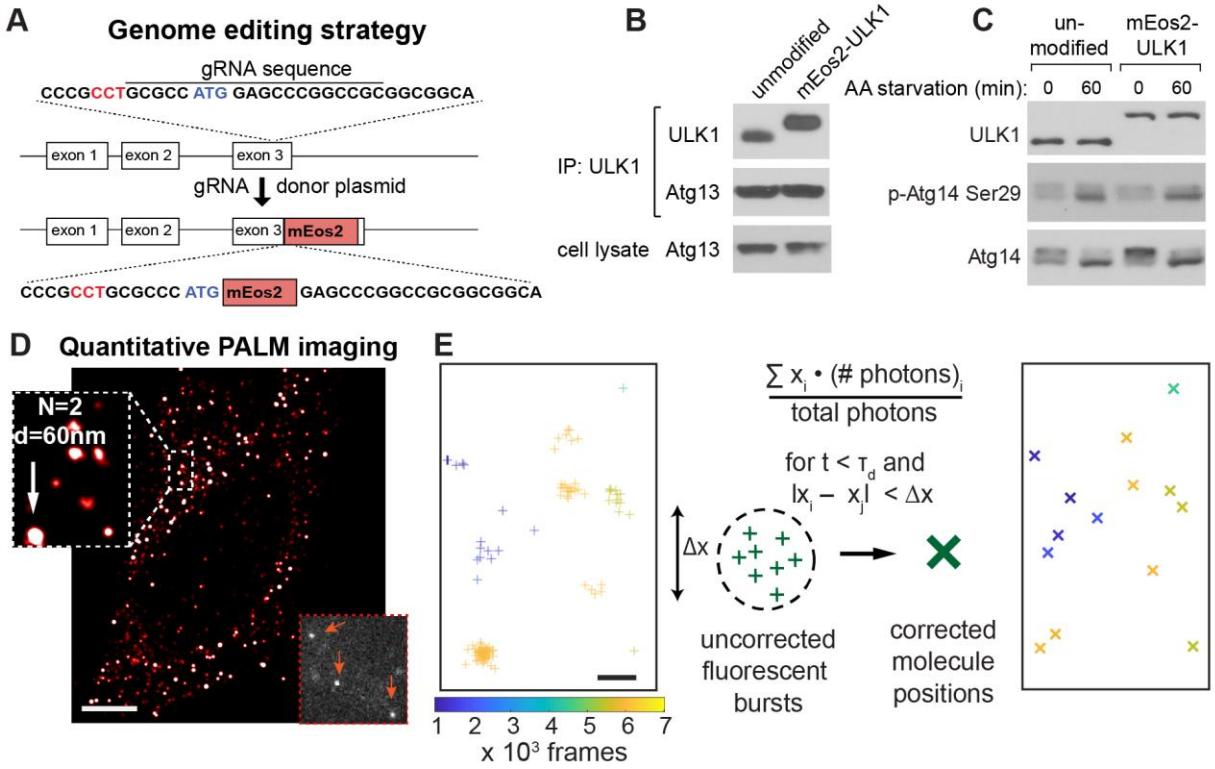

Fig. 1. **Quantifying the nanoscopic distribution and oligomeric state of endogenous ULK1 with qPALM**. (A) Schematics of endogenous tagging of ULK1 with mEos2. The PAM sequence of gRNA is depicted in red. The detailed procedure is described in Materials and Method section. (B) The endogenously tagged ULK1 interacts with Atg13 to the same degree as the untagged endogenous ULK1. Immunoprecipitates were obtained from HeLa cells modified in the genome (mEos2-ULK1) or unmodified HeLa cells using an anti-ULK1 antibody, and analyzed by western blotting for endogenous ULK1 and Atg13. (C) The endogenously tagged ULK1 is functionally intact for the activation of ULK1 in response to amino acid starvation. Cells were incubated in full medium (0) or amino acid starvation medium for 60 min. The degree of phosphorylation of Atg14 Ser29, an ULK1 target site (15), was analyzed by western blotting. (D) Rendered PALM image (red, scale bar 5 µm) shows the nanoscopic distribution of ULK1 oligomers throughout the cytoplasm. The bottom right inset shows bright single molecule fluorescence of mEos2-ULK1 in a single data acquisition frame. The zoom on the left exemplifies quantification of the size and oligomeric state of a ULK1 cluster. (E) Left: individual single molecule localizations are shown as crosses with a color code according to their frame of appearance. Some mEos2 molecules only appear in one frame and irreversibly bleach, whereas others blink multiple times and cause a cluster of localizations. Scale bar: 100 nm. Right: After averaging localizations appearing within the determined dark time cut-off and within the localization uncertainty, blinking of mEos2 was corrected and the number of ULK1 molecules was obtained.

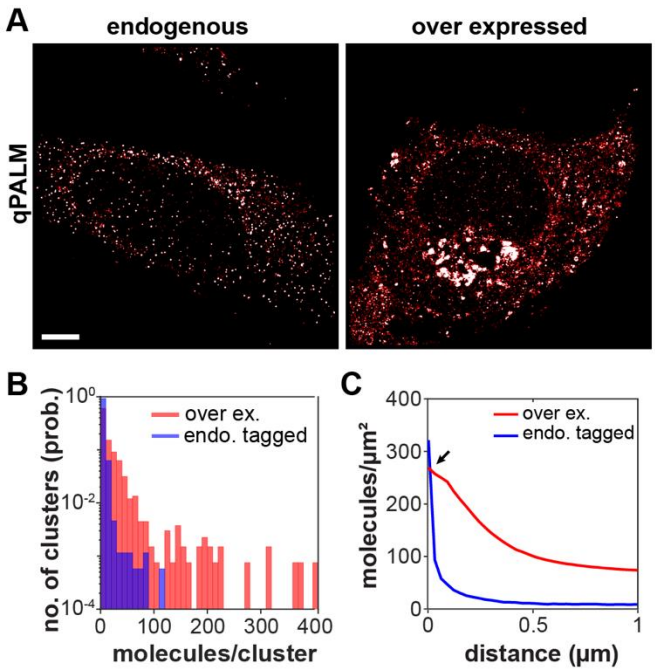

Fig.2. **Endogenous tagging of ULK1 is required to avoid artifacts in quantifying the nanoscopic distribution and oligomeric state of ULK1**. (A) qPALM images of endogenously tagged mEos2-ULK1 and overexpressed mEos2-ULK1 show that the overexpressed ULK1 forms highly dense structures, which might be clustering artifacts. (B) Analysis of qPALM data shows that overexpressed mEos2-ULK1 results in significantly more molecules and larger oligomers (red) than endogenously tagged mEos2-ULK1 (blue). (C) Radial distribution comparison between overexpressed and endogenously tagged ULK1 highlights differences in degree of ULK1 protein clustering. Overexpressed cells contain significantly larger cluster and a higher molecular densities at distances larger than 30 nm (arrow) but lower molecular densities at distances smaller than 30 nm when compared with endogenously tagged molecular clusters. Scale bars: 5 µm.

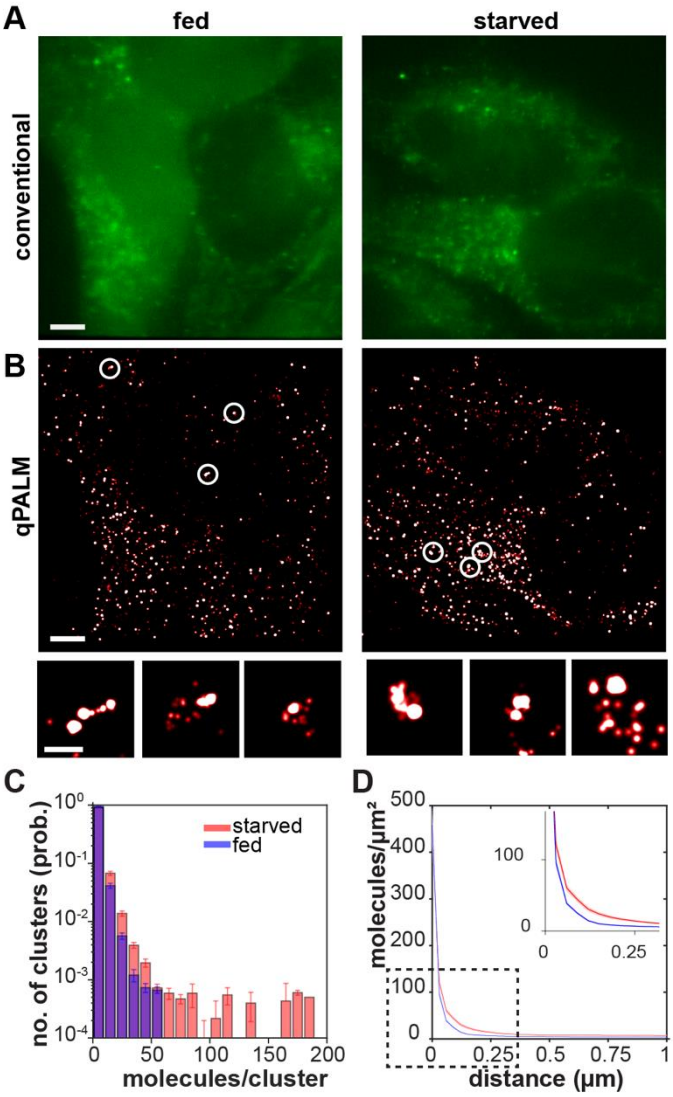

Fig. 3. **Amino acid starvation induces clusters with more ULK1 molecules and larger size**. (A) Conventional fluorescence images of mEos2-ULK1 in amino acid supplemented cells (fed) and amino acid deprived cells (starved) do not reveal a visual difference in the spatial distribution of ULK1. Scale bars: 5 µm. (B) Corresponding PALM images. Magnified regions show small diffraction-limited structures, which were impossible to be resolved in conventional fluorescence images. Scale bar: 500 nm. (C) The cluster analysis after the blink correction shows that amino acid starvation induced more higher-order oligomers containing up to 190 molecules (red) compared to fed cells (blue). The plot was generated by averaging the histogram of 19 fed and 23 starved cells, respectively. Error bars correspond to the standard error of the mean. (D) Averaged pair correlation function analysis of the cells from (C) shows an increase of cluster sizes in starved cells (red) compared to fed cells (blue).

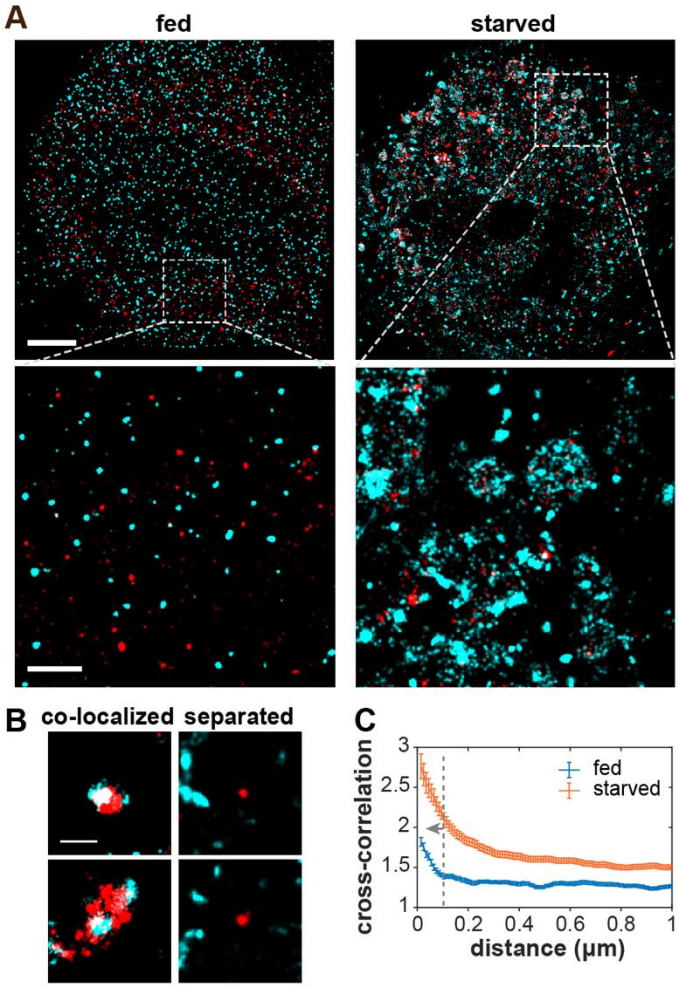

Fig. 4. **ULK1 clusters containing Atg13 display variability in size, shape, and multimeric state under starvation.** (A) Upper: Two-color overlay of PALM images of mEos2-ULK1 (red) and HaloTag-Atg13 bound with JF647 (cyan) in fed (left) and starved cells (right). Scale bar: 5 μm. Magnified images in the lower panel show the presence of various small dense clusters (lower left) and in addition arc-shaped and larger spherical structures that are only present in starved cells (lower right). Scale bar, 1 μm. (B) Magnification of two-color PALM images in starved cells show difference of ULK1 structures that do (left) and do not (right) co-localize with Atg13. ULK1 without Atg13 only forms small clusters, whereas ULK1 with ATG13 forms highly dense clusters and larger arc-shaped or spherical structures. Scale bar: 500 nm. (C) Cross-correlation of mEos2-ULK1(red) and Atg13-HaloTag JF646 (cyan) shows co-localization up to a distance of 100 nm between ULK1 and Atg13 in fed cells and a significantly larger degree of co-localization up to 200 nm in starved cells. The error bar corresponds to the standard error of the mean constructed from seven fed and ten starved cells.

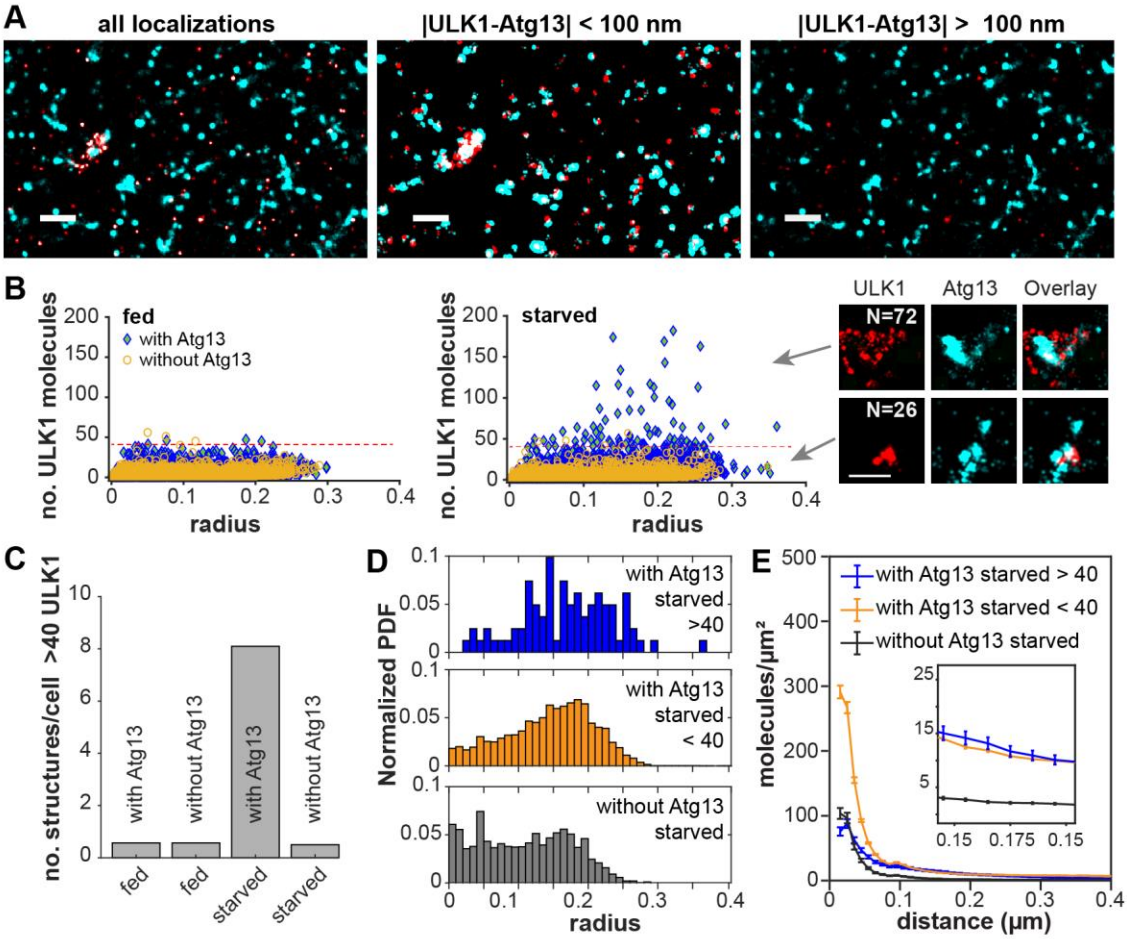

Fig.5. **Cross-correlation analysis of two-color PALM data identifies starvation induced structures containing Atg13 and up to 190 ULK1 molecules**. (A) Two-color PALM image of mEos2-ULK1 (red) and Atg13-HaloTag JF647 (cyan) in starved cells shows different clustering pattern of ULK1 in the close proximity to Atg13. Left: Grouping ULK1 an Atg13 based on the cross-correlation peak up to 100 nm in Fig. 4C (fed cells). ULK1 molecules and clusters within 100 nm separation of Atg13 form highly dense and larger arc- or spherical structures (middle), whereas ULK1 separated by more than 100 nm from Atg13 only forms small clusters. Scale bar: 1 µm. (B) Quantification of the oligomeric state and radius of ULK1 structures that are within a 100 nm distance of Atg13 (with Atg13, blue) compared to ULK1 structures not in proximity to Atg13 (without Atg13, orange). ULK1 structures with Atg13 show a slight increase in the number of ULK1 molecules but exhibit overall a similar distribution in fed cells compared to ULK1 without Atg13. (B, middle) The same quantification in starved cells shows small and dense ULK1 clusters with Atg13 as well as larger structures with up 190 ULK1 molecules that are neither formed by ULK1 molecules without Atg13 nor present in fed cells. The dashed line at 40 molecules indicates a threshold used for further analysis. The inset image exemplifies a large Atg13-containing structure with 72 ULK1 molecules as well as a small dense cluster with 26 molecules under starvation. Scale bar: 500 nm. (C) Number of structures with more than 40 ULK1 molecules per cell in different conditions. The number of each structure was quantified over 10 starved and 7 fed cells, and divided by the cell number for the graph presentation. (D) Normalized probability density function (PDF) of the radii of structures with more than 40 ULK1 molecules with Atg13, with more than 40 ULK1 molecules without Atg13 (middle), and all other ULK1

molecules without Atg13. (E) Radial distribution of ULK1 molecules on structures with more than 40 ULK1 molecules containing Atg13, with less than 40 ULK1 molecules containing Atg13 and all other ULK1 molecules without Atg13.

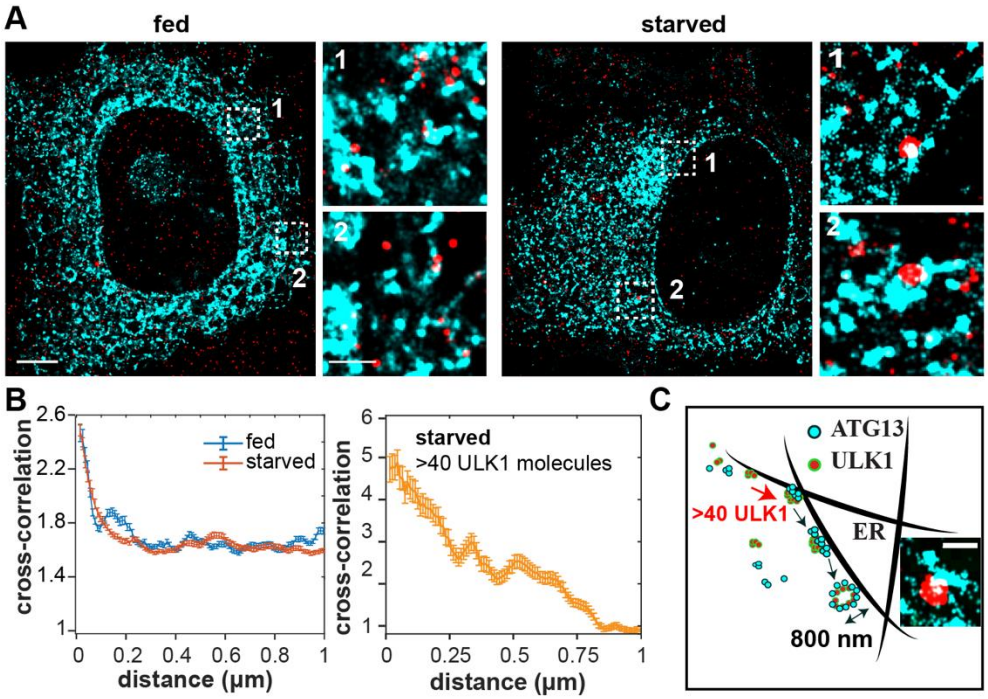

Fig.6. **Starvation induced structures with high numbers of ULK1 are in proximity to the ER**. (A) Two color PALM images of mEos2-ULK1 (red) and the ER marker HaloTag-Sec61β (cyan) in fed and starved cells. Upper scale bar, 5 μm. Zoom images of ULK1 and the ER show the presence of ULK1 clusters on or in close proximity to the ER in fed cells. Scale bar: 1 μm. In starved cells larger ULK1 structures with more than 40 ULK1 molecules are in contact or in proximity to the ER (lower right). (B) Cross-correlation plot of mEos2-ULK1 and HaloTag-Sec61β shows a similar co-localization of ULK1 to the ER in fed and starved cells. Structures containing more than 40 ULK1 molecules in starved cells exhibited a significantly larger degree of ER co-localization up to a longer distance. The peak with values >1 up to 800 nm distance indicates that ULK1 structures are at and near the ER. The value of 1 for distances > 800nm indicates that ULK1 is randomly distributed with respect to the ER. The shaded area corresponds to the standard error of the mean constructed from four individual starved cells. (C) Model of autophagosome initiation based on results. Upon starvation, small clusters of ULK1 which co-localize to some extent with Atg13 assemble on or near the ER and form highly dense clusters containing Atg13. These dense clusters with >40 ULK1 molecules then assemble to form larger arc-shaped structures, which might develop into phagophores. Phagophores eventually expand to form large spherical autophagosomes in proximity to the ER.